Kathuria, Abiad, Auras. Published in Polymer, 54(26). December 2013: 6967-6986.

# Toughening of poly(L-lactic acid) with $Cu_3BTC_2$ metal organic framework crystals

Ajay Kathuria [a,b], Mohamad G. Abiad [a,c], Rafael Auras [a,*]

[a] 448 Wilson Road, School of Packaging, Packaging Building Michigan State University, East Lansing, MI 48824-1223, USA
[b] 228 C, Jarvis Hall Technology Wing, College of Science, Technology, Engineering & Mathematics, University of Wisconsin-Stout, Menomonie, WI 54751, USA
[c] Department of Nutrition and Food Sciences, American University of Beirut, Beirut, Lebanon

A B S T R A C T

Poly(L-lactic acid) (PLLA) and metal organic framework (MOF) composites were prepared by melt extrusion of PLLA with 5, 10 and 20% w/w of activated $Cu_3(BTC)_2$ MOF. The morphology and stability of injection-molded samples were evaluated using thermogravimetric analysis, differential scanning calorimetry (DSC), gel permeation chromatography, X-ray diffraction, and scanning electron microscopy (SEM). The composites showed improved toughness during the tensile tests as compared to the neat PLLA matrix. Toughness mechanism of the composites was studied using SEM and rheological studies. SEM images indicated that cavitation induced by debonding at the interface of PLLA and MOF particles during the uniaxial stress was primarily responsible for the improved toughness of the composites. The SEM images of the composites, the solid like plateau observed in the PLLA composites during the parallel plate rheology at low frequency, and the decrease in the cold crystallization enthalpy during the developed composites indicate potential for various applications, which include gas separation, energy and active packaging.

## 1. Introduction

High petroleum prices, corporate environmental awareness and favorable legislations have provided an increase demand for bio-based and biodegradable polymers. Poly(lactic acid), PLA, the main commercially available bio-based and compostable polyester produced by the monomeric synthesis of L-lactic acid derived from renewable resources such as corn, cassava, or sugar beet has successfully gained market acceptance for consumer good applications [1,2]. PLA has similar mechanical, thermal and barrier properties like poly(styrene) and poly(ethylene terephthalate). It has high permselectivity to gases like ($CO_2/CH_4$) [3,4] so it has potential to be used for gas separation. However, the brittleness of PLA along with low heat deflection temperature and poor barrier properties hinders its wide market applications [5–7].

In general, fillers such as talc, carbon black and/or zeolites are added to polymeric matrix to reduce the cost or to achieve the desired properties like specific permselectivity. Mixed matrix membranes (MMMs), which traditionally consist of zeolite, carbon molecular sieves or other porous particles embedded in a polymeric matrix, are increasingly being used for improving mechanical properties, thermal properties and permselectivity of polymer [8–10]. Although MMMs prepared from inorganic materials like zeolites have been widely researched in the last few decades, the poor compatibility between the inorganic fillers and organic polymeric matrix can lead to sub-micron size holes in the MMMs [11,12]. Mahajan et al. [11] studied Matrimid™, a thermoplastic polyimide, with 20% zeolite 4A; they grafted the polyimide chains on the zeolite using silane coupling agent to improve compatibility between the zeolite 4A and Matrimid™.

Metal organic frameworks (MOFs) are a class of porous crystalline compounds manufactured from metal ions ($Cu^+$, $Cu^{2+}$, $Ag^+$, $Zn^{2+}$, $Co^{2+}$, $K^+$, etc.) bridged together by organic ligands forming multi-dimensional structures. MOFs offer a promising alternative to zeolites and other molecular sieves in the production of MMMs since they have high surface area, selective sorption, gas separation potential and storage capacity. However, high cost and poor mechanical properties of the MOF reduce possibility of commercial applications of these compounds. Incorporating MOFs in polymers is one the various solutions to contain the cost of membranes and achieve the desired mechanical properties. Hybrid inorganic–organic composition of the MOF compounds may offer better compatibility with organic polymeric material as compared to zeolites and other inorganic molecular sieves. Various researchers have synthesized MMMs using different MOFs and polymers to

* Corresponding author. Tel.: +1 517 432 3254; fax: +1 517 353 8999.
E-mail address: aurasraf@msu.edu (R. Auras).

improve the permeability and selectivity of the matrix [12–15]. Ploegmakers et al. [13] studied polyimide-copper benzene 1,3,5 tricarboxylate MOF MMMs for ethylene and ethane separation. They observed that 20% addition of $Cu_3BTC_2$ MOF in the polyimide increased the selectivity to ethylene/ethane of polyimide from 4.1 to 7.1. Scanning electronic microscopy images suggested good compatibility between polyimide and $Cu_3BTC_2$, and the glass transition temperature ($T_g$) of the polyimide decreased from 345 to 329 °C with the addition of 20% $Cu_3BTC_2$. Elangovan et al. [16] reported that PLLA and $Cu_3BTC_2$ MOF were compatible as determined by contact angle measurement offering improved composite characteristics like mechanical properties and selective barrier properties as compared to PLLA.

We have previously observed that strong polymer filler interactions played an important role in improving toughness of PLA-MOF composites [17]. Rheological studies can be helpful in understanding the complex microscopic interaction of polymeric chains with filler particles, which ultimately affects the macroscopic properties of the composites. Thus, the main purpose of this work was to understand the effect of the $Cu_3BTC_2$ MOF on the toughness, viscoelastic properties, morphology and stability of the PLA composites.

## 2. Methodology

### 2.1. Materials

Poly(L-lactic acid) (PLLA) resin grade 4043 D, 98% L-lactide, with weight average molecular weight ($M_w$), number average molecular weight ($M_n$) and polydispersity index ($M_w/M_n$) of 111 kDa, 84 kDa and 1.3; respectively, was provided by NatureWorks LLC (Blair, NE, USA). Basolite™ C300 MOF ($Cu_3BTC_2$) with surface area ranging from 1500 to 2100 $m^2\ g^{-1}$ and particle size ranging from 5 to 30 μm was purchased from Sigma Aldrich (St Louis, MO, USA).

### 2.2. Sample preparation

PLLA resin was dried at 80 °C for 4 h and Basolite™ C 300 MOF ($Cu_3BTC_2$) was activated at 200 °C for 24 h using a vacuum oven at 0.1 MPa. PLLA, PLLA–5% MOF, PLLA–10% MOF and PLLA–20% MOF composite samples were processed using a vertical co-rotating twin-screw micro-compounder (DSM Research, Geleen, The Netherlands) attached to an injection molder. The extruder has 150 mm screw long screws with $L/D$ ratio of 18. The volume of the barrel is ~15 $cm^3$. The material was processed at 190 °C using 5 min cycle time at ~1 MPa (140 psi) injection pressure. The transfer cylinder and mold temperatures were set at 195 and 65 °C, respectively. Dogbone tensile bars, flexural samples, and X-ray diffraction (XRD) discs of PLLA, PLLA–5% MOF, PLLA–10% MOF and PLLA–20% MOF composites were prepared and stored in a desiccator at room temperature (~23 °C) until further testing.

### 2.3. Characterization

#### 2.3.1. Tensile test

Tensile properties were evaluated according to ASTM D638-10 using a Universal Tensile Machine model UTS SFM 20 from United Calibration Corporation, (Huntington Beach, CA, USA). The machine was equipped with a laser extensometer. Injection molded dogbone samples with a gauge length of 25.4 mm were stored at room temperature in a dessicator over desiccant for at least 40 h prior to testing. The samples were then tested at room temperature (~23 °C) using a 453 kg load cell at 0.023 kg of preload. PLLA, PLLA–5% MOF, PLLA–10% MOF and PLLA–20% MOF were tested at a crosshead speed of 50.8 mm $min^{-1}$ (2 in/min).

#### 2.3.2. Rheology

Dynamic frequency sweep tests of PLLA and PLLA composites were performed using AR 2000 advanced rheometer from TA-Instruments (New Castle, DE, USA) at 175 °C using 25 mm diameter parallel plates with a gap of 1100 μm and frequency ranging from 0.01 to 100 rad/s. The strain used for the frequency sweep tests was selected as 2%, which is in the linear viscoelastic range of the material as determined by strain sweep.

#### 2.3.3. X-Ray diffraction (XRD)

X-Ray diffraction spectroscopy was performed on XRD discs of PLLA, PLLA–5% MOF, PLLA–10% MOF and PLLA–20% MOF stored at 23 °C using a Bruker D8 advance X-ray diffractometer (Bruker AXS GmbH, Karlsruhe, Germany) at 40 kV, 40 mA (1600 W) using Cu Kα radiation ($\lambda$ = 1.5418 Å). The studies were conducted using a 1.2 mm primary beam slit and 2.0 mm detector slit. The X-ray scans were carried out at speed of 0.02° per second. Data was collected in triplicates.

#### 2.3.4. Differential scanning calorimetry (DSC)

A DSC Q100 (TA instruments) was used to perform DSC analysis using heat/cool/heat cycles from 0 to 180 °C at a rate of 10 °C $min^{-1}$. The melting temperature ($T_m$) and the associated heat enthalpy ($\Delta H_m$) were calculated from the first heating cycle. The glass transition ($T_g$) temperature, cold crystallization onset ($T_{co}$), cold crystallization peak ($T_{cc}$) and enthalpy of cold crystallization ($\Delta H_c$) were calculated from the second heating cycle to eliminate any thermal history, which may have been introduced during processing or storage. The samples were run in triplicates.

Consequently, the percent crystallinity of the samples was estimated using equation (1):

$$X_c(\%) = \frac{\Delta H_m - \Delta H_c}{\Delta H_m^c (1 - x)} \times 100 \quad (1)$$

where $\Delta H_m$ is the enthalpy of fusion; $\Delta H_c$ is the enthalpy of cold crystallization; $\Delta H_m^c$ is the enthalpy of fusion of pure crystalline PLA; $\Delta H_m^c = 93.1$ J/g [18]; and $x$ is the mass fraction of the MOF in the MMM.

#### 2.3.5. Thermogravimetric analysis (TGA)

Thermogravimetric analysis of $Cu_3BTC_2$ MOF, PLLA, PLLA–5% MOF, PLA–10% MOF and PLA–20% MOF was performed using a TGA 2950 (TA-Instruments, New Castle, DE, USA) under nitrogen flow of 100 ml/min. Samples weighing between 5 and 10 mg were heated at a rate of 10 °C/min from 25 °C to 700 °C. The data was analyzed using the Universal Analysis software version 2000 (TA Instruments, New Castle, DE, USA). The TGA samples were run in triplicates.

#### 2.3.6. Weight average molecular weight

To study the effect of processing conditions and MOF content on the stability of the PLLA, gel permeation chromatography (GPC) analysis were performed on the PLLA resin, extruded PLLA and PLLA–MOF composites using a GPC by Waters Inc. (Milford, MA, USA). Calibration was done using polystyrene standard materials with a molecular weight ranging from $2.9 \times 10^3$ to $3.64 \times 10^6$ Da using a third order polynomial equation. The analyses were performed at a flow rate of 1 mL/min and runtime of 45 min at 35 °C using the Mark–Houwink corrected constant $K = 0.000174$ (mL/g) and $a = 0.736$ for dilute PLLA solution in tetrahydrofuran (THF) [19]. The instrument was equipped with a Waters 1515 isocratic pump, Waters 717 autosampler, a series of Waters Styragel Columns (HR4, HR3 and HR2) and Waters 2414 refractive index. Approximately 20 mg of specimen were dissolved in 10 mL of HPLC grade THF with

99.99% purity (Pharmco-Aaper, Brookfield, CT, USA). The solution was then filtered using a 0.45 μm filter.

*2.3.7. Scanning electron microscopy (SEM)*

To understand the morphology of the composites, gold coated samples sputtered using an Emscope SC 500 (Emscope Laboratories Ltd., Ashford, UK) were analyzed using a JEOL JSM 6610 LV (JEOL, Japan) scanning electron microscope (SEM) at 12 kV accelerating voltage. The microscope was equipped with a tungsten filament.

*2.3.8. Data analysis*

Tukey's HSD (Honestly Significant Differences) tests were performed to determine if the means were significantly different from each other at 95% confidence interval ($\alpha = 0.05$). The analyses were conducted using SAS 9.0 Software (SAS Institute Inc., Cary, NC, USA).

## 3. Results and discussion

### 3.1. Tensile test/toughness

Craze formation is primarily responsible for the brittle failure of PLA under tensile stress. The low entanglement density of amorphous glassy PLA favors crazing over shear yielding leading to a brittle fracture [20–22]. The toughness of the PLA can be improved by various methodologies such as the addition of impact modifying rubber particles, inorganic particles, blending, plasticization, etc. [22–26]. In heterogeneous matrix the organic/inorganic particles or other fillers serve as stress concentrators [27–30]. Good interfacial interactions between the particles and the matrix are a prerequisite to achieve better mechanical properties. Under uniaxial stress, the triaxial stress generated at the interface of the filler particles and the organic matrix can promote debonding and cavitation. Debonding at the interface releases the triaxial stress and cavitation triggered matrix-shearing can dissipate the energy leading to the plastic deformation and improved toughness of the composite materials. A schematic representation of the cavitation process is presented in Fig. 1.

Tensile properties of PLLA and PLLA-MOF composites are summarized in Table 1. Stress strain graph of PLLA, PLLA–5% MOF, PLLA–10% MOF and PLLA–20% MOF composites can be observed in Fig. 2. Brittle fracture was observed for PLLA matrix without any

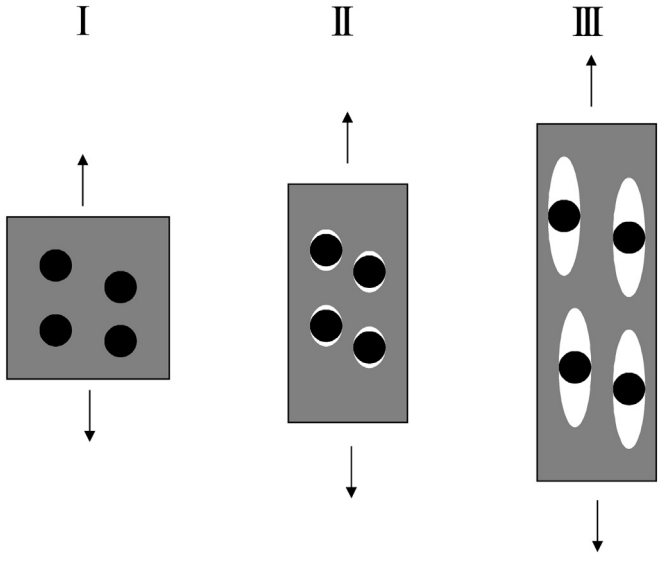


**Fig. 1.** Toughening mechanism of PLLA–MOF composites adapted from Refs. [28,30], step I: polymer MOF composite, step II: debonding at the interface of the polymer–MOF interface under tensile stress, step III: plastic deformation.

**Table 1**
Tensile properties of PLLA, PLLA–5% MOF, PLLA–10% MOF and PLLA–20% MOF.

| Material | Tensile strength (MPa) | Elongation at break (%) | Modulus of elasticity (GPa) | Toughness ($MJ/m^3$) |
|---|---|---|---|---|
| PLLA | $76.9 \pm 1.5^{A}$ | $3.6 \pm 1.5^{A}$ | $3.0 \pm 0.3^{A}$ | $1.70 \pm 1.06^{A}$ |
| PLLA–5% MOF | $58.9 \pm 0.8^{B}$ | $16.9 \pm 3.2^{B}$ | $3.0 \pm 0.2^{A,B}$ | $8.49 \pm 1.45^{B}$ |
| PLLA–10% MOF | $52.4 \pm 1.2^{C}$ | $9.8 \pm 3.9^{C}$ | $2.8 \pm 0.1^{A,B}$ | $4.33 \pm 1.86^{C}$ |
| PLLA–20% MOF | $44.5 \pm 0.1^{D}$ | $5.4 \pm 1.4^{A,C}$ | $2.6 \pm 0.2^{B}$ | $1.86 \pm 0.51^{A,C}$ |

Values in the same column with the same capital superscript letters are not statistically significantly different at $\alpha = 0.05$.

plastic deformation. However, PLLA–MOF composites showed considerable plastic deformation especially for PLLA–5% MOF composites. Tensile force generated stress concentration at the interface of matrix and the $Cu_3BTC_2$ MOF led to debonding initiated cavitation process at the interface of MOF particles and PLLA matrix as observed in SEM micrographs represented in Fig. 3b–d [29–31]. The stress generated by tensile force at room temperature was diffused around the voids, generating local plastic deformation followed by strain softening. The decrease in the yield stress of the composites can be ascribed to the dilative stress component, which decreases the yield stress or the onset of the plastic deformation [32,33]. The yield stress decreased with the increase in the MOF concentration from 5 to 20% due to increased dilatation with increased MOF concentration under tensile stress although minimal changes in the modulus of elasticity were observed [33–35]. Orientation, geometry and aspect ratio of the filler play a critical role in determining the final properties of the composites [36]. MOFs are isotropic particles and can be compared to spheroidal particles with low aspect ratio ($\alpha = 1$). The low aspect ratio and micro-size of the particles are both responsible for the minor change in the modulus of elasticity. Parsons et al. [37] also observed increased dilatation with increase in the $CaCO_3$ concentration from 10 to 20% in HDPE matrix. Wu [38] studied toughening of polymer using rubber particles. The authors concluded that interparticle distance (matrix ligament thickness) is a crucial factor for the toughening effect due to cavitation. This effect was primarily due to yielding of the ligament. We observed decrease in the elongation of the composites with increase in the concentration from 5 to 20%. The matrix ligaments present between the induced cavities are primarily responsible for the increase in toughness. In the case of PLA–5% MOF composites, the ligament has the critical thickness (or critical interparticle distance) needed for the tough–brittle transition. However, an increase in MOF

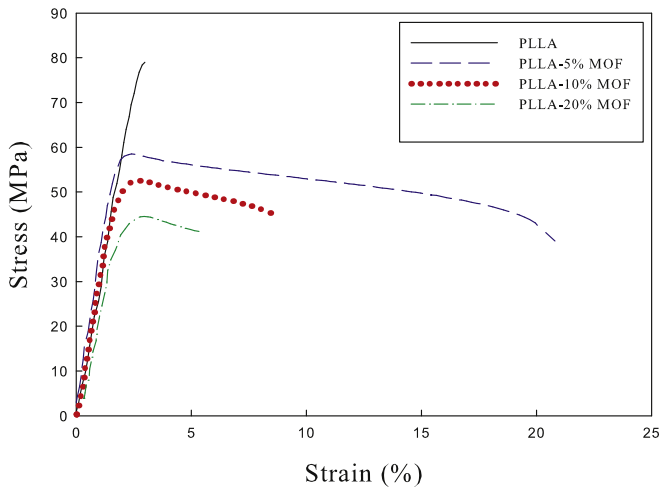


**Fig. 2.** Stress strain graph of PLLA and PLLA MOF composites.

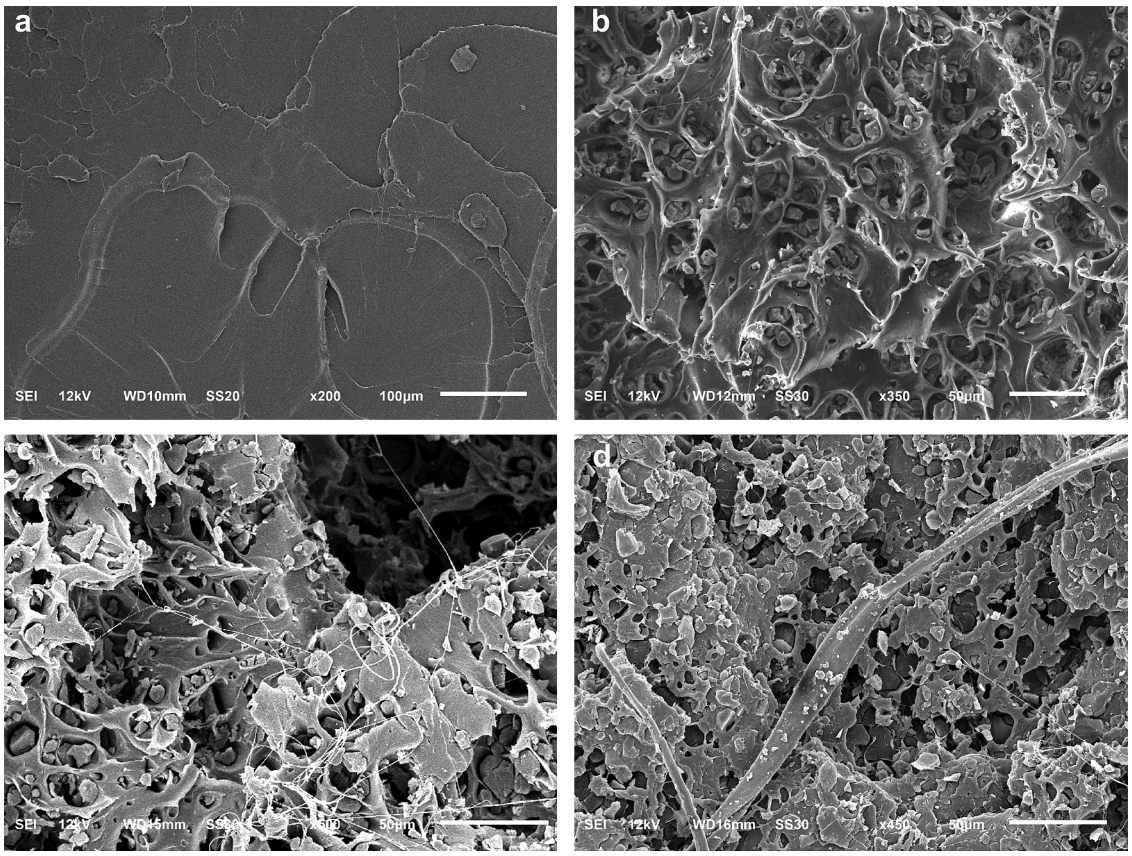


**Fig. 3.** Tensile fractured cross-section of a. PLLA, b. PLLA−5% MOF, c. PLLA−10% MOF, d. PLLA−20% MOF.

concentration diminishes the distance between cavities created by two neighboring particles. Consequently, under uniaxial stress the cavities propagate to macro-defect without much resistance from the matrix leading to a brittle failure [35]. The bigger size cavities are easily visible in microscopic images of PLLA−20% MOF composition in Fig. 3d.

Several researchers have studied surface modified or coated inorganic particles [24,28,31]. Meng et al. [31] fabricated PLA composites with nano-titania particles and nano-titania particles coated with polycaprolactone (PCL) in various concentrations ranging upto 40%. The authors reported significant improvement in the toughness of the PCL coated nano-titania composites due to debonding at the interface and cavitation process. Improved toughness was also attributed to the even distribution of stress around the interface of the matrix and uniformly dispersed fillers in the heterogeneous systems. The maximum strain at break of 64.7% was achieved at 26.5 wt.% loading of coated $TiO_2$. On the other hand, in PLA uncoated $TiO_2$ composites, the $TiO_2$ particles agglomerated, leading to insignificant improvement in the mechanical properties. Zuiderduin et al. [28] studied the effect of $CaCO_3$ and steric acid modified $CaCO_3$ particles on the toughening of polypropylene. Steric acid modified $CaCO_3$ particles dispersed well and provided good mechanical properties, while partial agglomeration was observed in $CaCO_3$ particle especially at higher concentration, which led to brittle transition. Above 40 wt% $CaCO_3$ particles, a brittle failure was observed due to agglomeration. Glassy thermoplastics undergo plastic deformation in pure shear [39]. In the plastic deformation region the decrease in the tensile strength with the increase in the strain could be related to the increase in the shear flow with the increase in the void size.

### 3.2. Rheological studies

The storage modulus ($G'$), loss modulus ($G''$), and tan $\delta$ ($G''/G'$) of PLLA, PLLA−5% MOF, PLLA−10% MOF, and PLLA−20% MOF as a function of oscillatory frequency are represented in Fig. 4a−c; respectively. The storage modulus of PLLA follows typical entangled polydisperse melt. A secondary plateau or terminal shoulder was observed at low frequencies the PLLA−MOF composites $G'$ plots. This solid like behavior can be ascribed to the three dimensional network formation [21,40,41] caused by bridging of the strong polymeric chain between the MOF particles due to strong PLLA−$Cu_3BTC_2$ MOF interactions [17]. These topological restraints may have contributed towards the immobilization of the polymeric chains in the PLLA−MOF composites limiting their ability to relax at low frequency. This observation was also supported by DSC studies discussed later in this paper. At high frequency the polymeric chains were able to overcome these restraints as represented in Fig. 5 [41].

Tan $\delta(G''/G')$ of PLLA and PLLA composites as a function of frequency sweep is represented in Fig. 4c. The tan $\delta$ showed a decreasing trend with increasing frequency in case of PLLA. However, mild peaks were observed for the PLLA−MOF composites around 0.5 rad $s^{-1}$.

Fig. 4d represents the complex viscosity ($\eta^*$) of the PLLA, PLLA−5% MOF, PLLA−10% MOF and PLLA−20% MOF composites. The decrease in complex viscosity of the composites as compared to PLLA may be attributed to the free volume change and the decrease in the entanglement. Similar observations were made by other researcher during the fabrication of composites with modified inorganic particles [42,43]. Luo et al. [42] studied composites of PLA and $TiO_2$ functionalized with lactic acid. They observed decrease in the complex viscosity with the addition of the functionalized $TiO_2$.

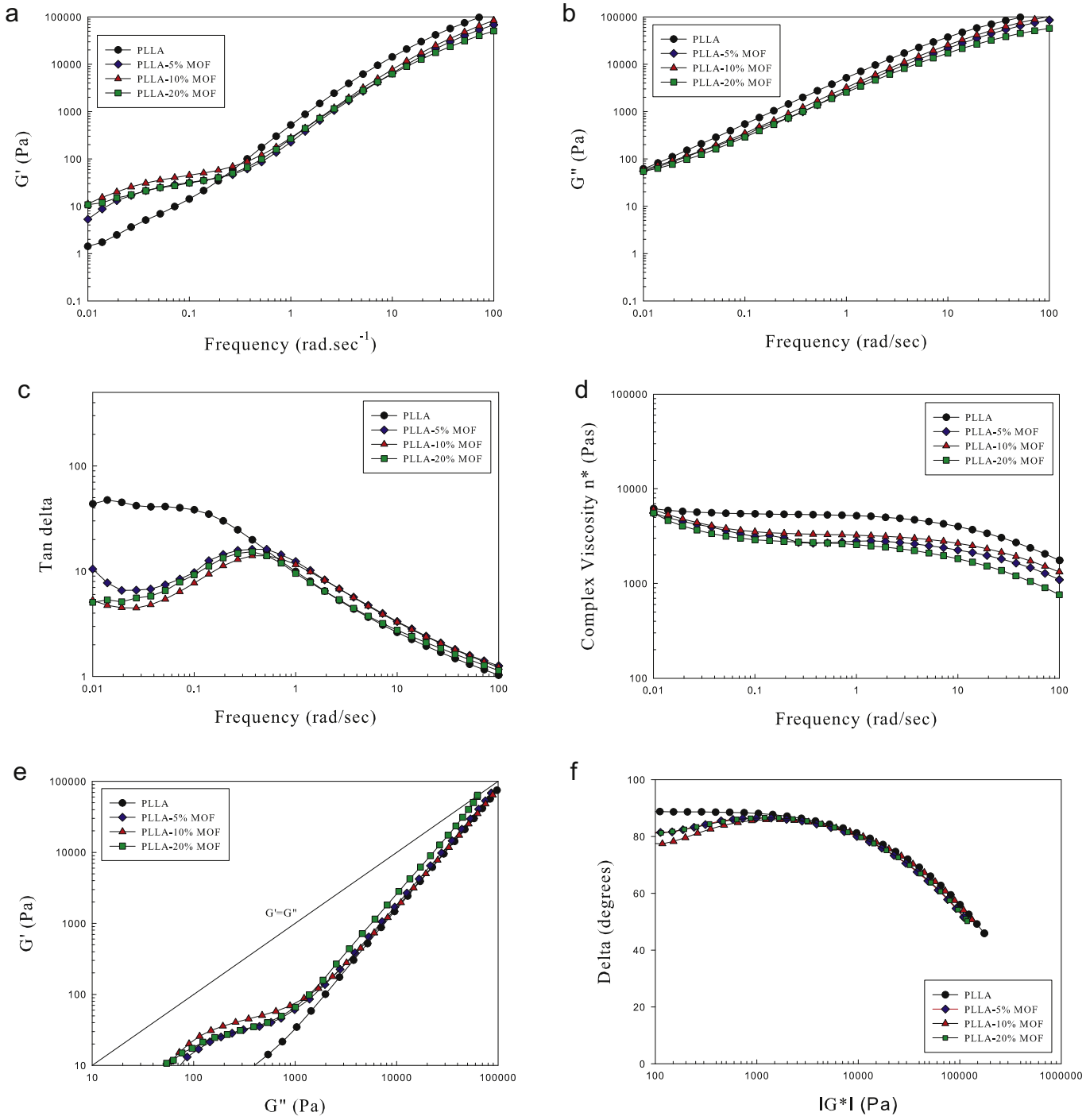


**Fig. 4.** a) Storage modulus ($G'$) of PLLA and PLLA MOF composites as a function of oscillatory frequency, b) loss modulus ($G''$) of PLLA and PLLA MOF composites as a function of oscillatory frequency, c) tan $\delta$ curves of PLLA and PLLA–MOF composites, d) complex viscosity of PLLA and PLLA MOF composites, e) Cole Cole plot of PLLA and PLLA MOF composites, f) Van Gurp Palmen plot of PLLA and PLLA MOF composites.

The authors attributed the decrease in the complex viscosity to the decrease in entanglement of linear polymeric chains. Lin et al. [43] observed 40% decrease in the complex viscosity of PLA–2.5% hyperbranched polyester amide blend as compared to PLA, further decrease in the complex viscosity was observed with increasing hyperbranched polyester amide content up to 15% which was inferred to the increase in the free volume and decrease in the entanglements.

A Cole–Cole plot of the PLLA, PLLA–5% MOF, PLLA–10% MOF and PLLA–20% MOF is represented in Fig. 4e. $G'$ and $G''$ represent the elastic and viscous parts of the complex viscoelastic fluids. At low frequencies, the viscoelastic properties are very sensitive and indicative of the underlying molecular architecture of the structure. At 175 °C PLLA primarily demonstrated viscous behavior than the elastic behavior. However, with the addition of MOF particles the elastic component of the PLLA increased at low frequency with increasing MOF content due to favorable interactions between PLLA matrix and the MOF crystals.

The van Gurp–Palmen plot of PLLA, PLLA–5% MOF, PLA–10% MOF and PLLA–20% MOF composites is represented in Fig. 4f. The

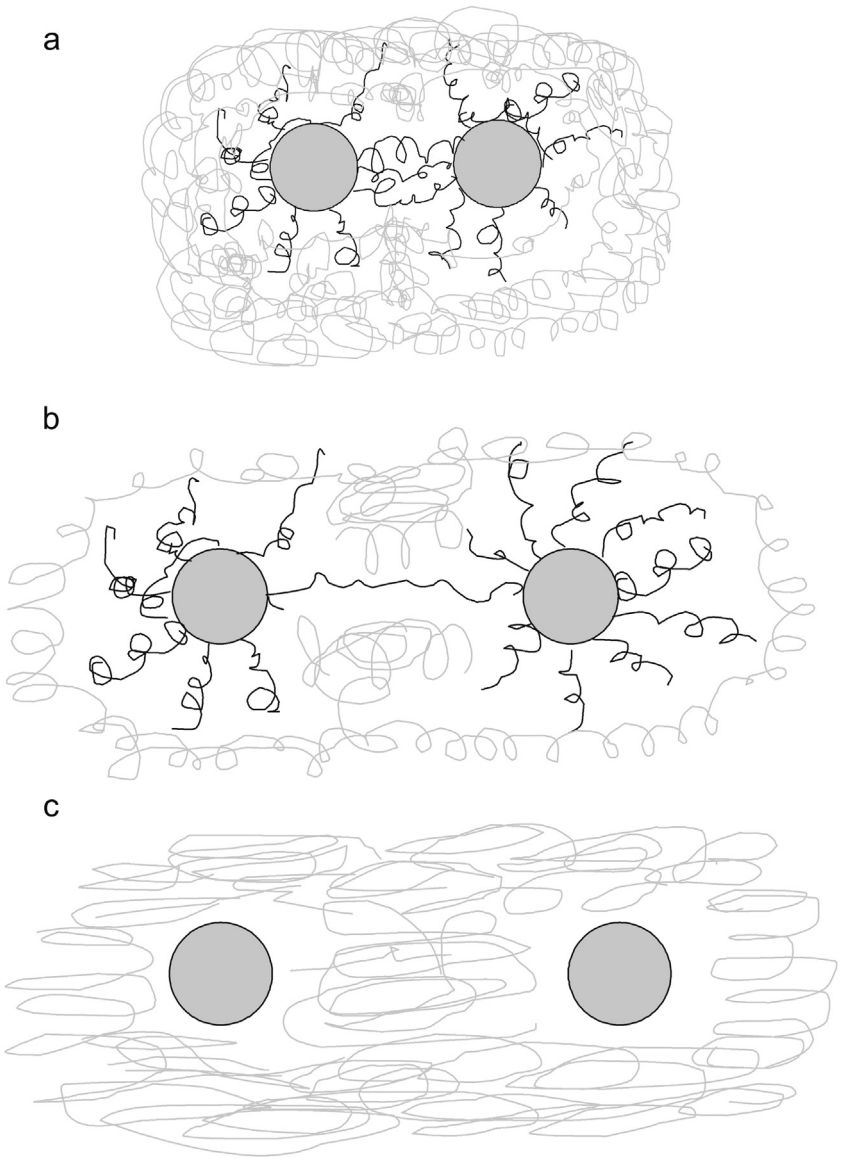


**Fig. 5.** Schematic representation of the configuration of polylactide MOF composites a. at rest, b. low shear rates, c. at high shear rates [41].

high phase angle of the composites at low frequency indicates that the composites were free of percolation. PLLA curve approaching phase angle close to 90° also indicates primarily viscous behavior. The addition of $Cu_3BTC_2$ MOF crystals provides minor improvement in elastic behavior, which increases with the increase in the MOF concentration from 5 to 20%.

### 3.3. X-Ray diffraction (XRD)

Diffraction patterns of PLLA, PLLA−5% MOF, PLLA−10% MOF and PLLA−20% MOF composites are represented in Fig. 6. The wide PLLA hump suggests amorphous nature of injection molded PLLA samples. In case of composites we can see the crystalline peaks of metal organic framework at the top of amorphous PLLA background. During extrusion process PLLA composites retained their face centered cubic (FCC) crystal structure. In a previous study [17], we observed that the adsorption of water by MOF particles before extrusion was detrimental to the final properties of the composites. Detailed analysis on the effect of heat and moisture on the $Cu_3BTC_2$ MOF crystal structure during extrusion with PLLA is presented elsewhere [17].

### 3.4. Differential scanning calorimetry (DSC)

The average crystallization onset temperatures for PLLA, PLLA−5% MOF, PLLA−10% MOF and PLLA−20% MOF observed in the DSC studies were 103.8, 113.8115.1 and 115.2 °C, respectively. Shift in the onset of cold crystallization temperature of the PLLA−MOF composites to the higher temperatures with the increase in the MOF content can be attributed to the good interactions between the polymeric chains and MOF crystals, which hindered the mobility of the chain. Such interactions between the polymeric chains and MOF crystals support the finding of the increase in the shear storage modulus in the rheology studies in the terminal region as observed in Fig. 4a. Table 2 represents the detailed DSC analysis of PLLA and its composites. We can also observe that the cold crystallization enthalpy decreased with the addition of the MOF. The decreased mobility of the polymeric chains is attributed to the strong interactions between the $Cu_3BTC_2$ MOF crystals and PLLA. There was no significant change in the $T_g$ of the composites as compared to PLLA, which indicates that the addition of the MOF crystals does not provide any flexibility to the chain.

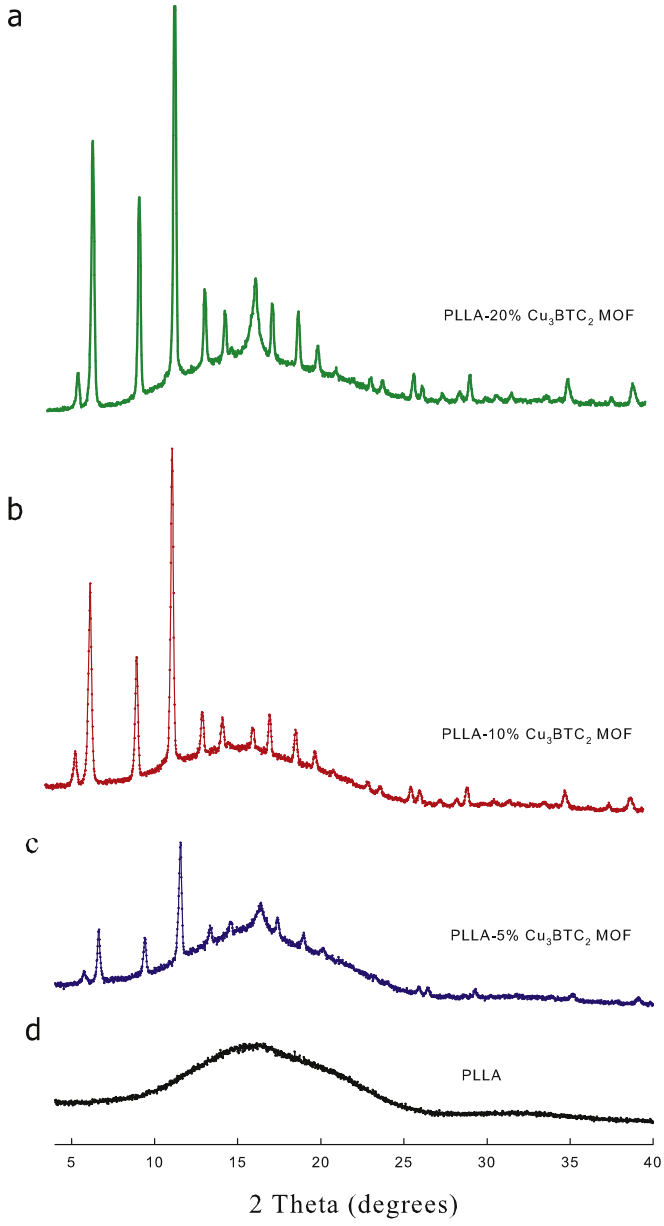


**Fig. 6.** X Ray diffraction patterns of PLLA–MOF composites.

### 3.5. Thermogravimetric analysis (TGA)

The TGA thermographs for activated MOF, PLLA, PLLA–5% MOF, PLLA–10% MOF and PLLA–20% MOF are represented in Fig. 7. The activated MOF has 5% w/w moisture content mostly adsorbed during the loading of sample into the machine. The organic component of the framework, benzene tricarboxylate, starts degrading at around 325 °C. The average onset of thermal degradation of PLLA, PLLA–5% activated MOF and PLLA–10% activated MOF and PLLA–20% MOF starts at 324.5, 322.5, 320.5 and 315.8 °C respectively. The increase in the concentration of MOF decreases the onset of thermal degradation of the composites. We observed $T_d$ for PLLA around 385 °C where as the PLLA–MOF composites have $T_d$ around 500 °C; respectively. It could be ascribed to the conversion of the remaining benzene tricarboxylate groups present in the MOF to CO and $CO_2$ as observed by Huang et al. in their ReaxFF reactive molecular dynamics (RMD) simulation studies [44]. They observed that $Cu_3BTC_2$ MOF has good thermal stability up to 300 °C, at higher temperatures the structural collapse of MOF has been simulated [44]. The difference in the final plateau for the PLLA, PLLA–5% MOF, PLLA–10% MOF and PLLA–20% MOF is mainly attributed to the difference in the metal content in the composites.

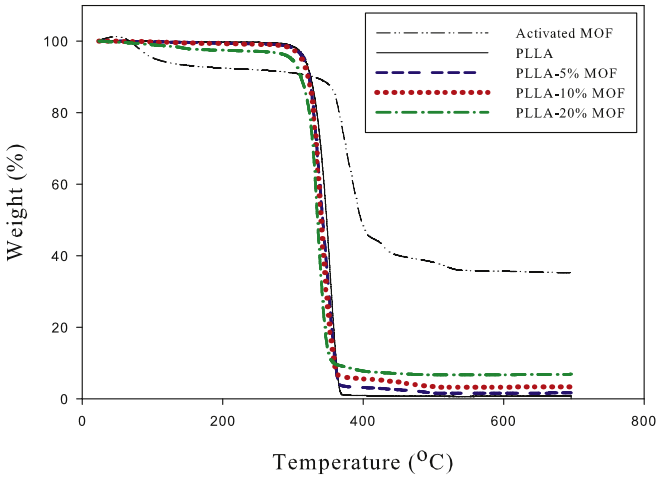


**Fig. 7.** Thermogravimetric analysis of PLLA, $Cu_3BTC_2$ MOF and PLLA MOF composites.

### 3.6. Gel permeation chromatography (GPC)

GPC analysis was performed on PLLA, PLLA–5% MOF, PLLA–10% MOF and PLLA–20% MOF. Table 3 shows the $M_w$, $M_n$, and PDI data of PLLA, PLLA–5% MOF, PLLA–10% MOF and PLLA–20% MOF. No statistically significant difference in the PLLA and PLLA MOF composites was found indicating that the presence of MOF does not degrade PLA and not residual water was presented during the composite production.

## 4. Conclusions

The PLLA–hybrid MOF composites were prepared by the melt extrusion process. The uniformly dispersed MOF particles in the polymer matrix increased the toughness of PLLA matrix by debonding initiated cavitation process. Large plastic deformation was observed for PLLA–5 wt.% of $Cu_3BTC_2$ MOF. Favorable

**Table 2**
Detailed DSC analysis information of PLA and its composites.

| Sample | $T_g$ (°C) | Cold crystallization | | | Melting | | |
|---|---|---|---|---|---|---|---|
| | | $T_{co}$ (°C) | $T_{cc}$ (°C) | $\Delta H_c$ (J/g) | $T_{mo}$ (°C) | $T_m$ (°C) | $\Delta H_m$ (J/g) |
| PLLA | $60.8 \pm 0.1^{A}$ | $103.8 \pm 0.2^{A}$ | $119.1 \pm 0.1^{A}$ | $19.6 \pm 0.9^{A}$ | $143.3 \pm 0.1^{A}$ | $147.9 \pm 0.2^{A}$ | $21.9 \pm 0.5^{A}$ |
| PLLA–5% MOF | $60.9 \pm 0.0^{A}$ | $113.8 \pm 0.2^{B}$ | $129.9 \pm 0.4^{B}$ | $3.6 \pm 0.1^{B}$ | $145.5 \pm 0.1^{B}$ | $150.8 \pm 0.1^{B}$ | $6.9 \pm 0.3^{B}$ |
| PLLA–10% MOF | $62.8 \pm 0.0^{B}$ | $115.1 \pm 1.1^{B}$ | $131.2 \pm 1.2^{B}$ | $5.6 \pm 1.4^{B,C}$ | $145.8 \pm 0.8^{B}$ | $152.9 \pm 1.0^{B}$ | $11.0 \pm 0.7^{C}$ |
| PLLA–20% MOF | $62.2 \pm 0.3^{C}$ | $115.2 \pm 0.4^{B}$ | $129.7 \pm 0.1^{B}$ | $6.7 \pm 0.3^{D}$ | $145.4 \pm 0.5^{B}$ | $152.2 \pm 1.3^{B}$ | $15.0 \pm 2.5^{D}$ |

Values in the same column with the same capital superscript letters are not statistically significantly different at $\alpha = 0.05$.

**Table 3**
Molecular weight of PLLA, PLLA−5%-MOF, PLLA−10% MOF and PLLA−20%-MOF.

| | PLLA control | PLLA−5% MOF | PLLA−10% MOF | PLLA−20% MOF |
|---|---|---|---|---|
| $M_n$, kDa | $71.9 \pm 1.2^{A}$ | $72.8 \pm 3.1^{A}$ | $73.4 \pm 0.6^{A}$ | $71.7 \pm 3.8^{A}$ |
| $M_w$, kDa | $103.0 \pm 0.7^{A}$ | $102.7 \pm 1.2^{A}$ | $102.2 \pm 0.2^{A}$ | $107.1 \pm 1.7^{B}$ |
| PDI | $1.4 \pm 0.0^{A,B}$ | $1.4 \pm 0.0^{A,B}$ | $1.4 \pm 0.0^{B}$ | $1.5 \pm 0.1^{A}$ |

Values in the same column with the same capital superscript letters are not statistically significantly different at $\alpha = 0.05$.

interfacial interactions necessary between $Cu_3BTC_2$ MOF and PLLA for improved toughening were further endorsed by rheological, microscopy studies and thermal analysis (DSC studies). Strong interactions between MOF particles and PLLA restrict the mobility of the polymeric chains. The MOF crystals retained their structure during extrusion processing as observed in the XRD studies. Gel permeation chromatography indicated that processing of PLLA with MOF did not have any significant effect on the molecular weight of the polymer in the final MMMs compositions.

## Acknowledgments

The authors would like to thank Rahul Bhardwaj, MeadWestVaco Corp. and Edward Drown, Composite Materials and Structures Center, Michigan State University for their constructive and useful comments. The authors are also thankful to Krishnamurthy Jayaraman, Chemical Engineering and Material Science at MSU for allowing the use of his laboratory for rheological studies. The authors would also like to thank Carol Fledgler and Abigail Tirrell from the Center for Advance Microscopy at MSU for their support.

## References

[1] Auras R, Harte B, Selke S. Macromol Biosci 2004;4:835−64.
[2] Soto-Valdez H, Auras R, Peralta E. J Appl Polym Sci 2011;121:970−8.
[3] Weber CJ, Haugaard V, Festersen R, Bertelsen G. Food Addit Contam 2002;19:172−7.
[4] Almenar E, Auras R. In: Auras R, Lim LT, Selke SEM, Tsuji H, editors. Permeability, sorption and diffusion of pure PLA in poly(lactic acid) synthesis, structures, properties, processing, and applications. Wiley Series; 2010.
[5] Auras R, Harte B, Selke S, Hernandez R. J Plast Film Sheet 2003;19:123−35.
[6] Auras R, Harte B, Selke S. J Appl Polym Sci 2004;92:1790−803.
[7] Teng CC, Ma CCM, Cheng BD, Shih YF, Chen JW, Hsiao YK. Compos Part A Appl Sci 2011;42:928−34.
[8] Chung TS, Jiang LY, Kulprathipanja S. Prog Polym Sci 2007;32:483−507.
[9] Husain S, Koros WJ. J Membr Sci 2007;288:195−207.
[10] Pechar TW, Kim S, Vaughan B, Marand E, Tsapatsis M, Jeong HK, et al. J Membr Sci 2006;277:195−202.
[11] Mahajan R, Koros WJ. Polym Eng Sci 2002;42:1420−31.
[12] Adam R, Carson C, Ward J, Tannenbaum R, Koros W. Microporous Mesoporous Mater 2010;131:13−20.
[13] Ploegmakers J, Japip S, Nijmeijer K. J Membr Sci 2013;428:445−53.
[14] Perez EV, Balkus KJ, Ferraris JP, Musselman IH. J Membr Sci 2009;328:165−73.
[15] Basu S, Cano-Odena A, Vankelecom IFJ. J Membr Sci 2010;362:478−87.
[16] Elangovan D, Yuzay I, Selke S, Auras R. Polym Int 2012;61:30−7.
[17] Kathuria A, Abiad MG, Auras R. Polym Int 2013;62:1144−51.
[18] Inkinen S, Hakkarainen M, Albertsson A, Södergard A. Biomacromolecules 2011;12:523−32.
[19] Dorgan JR. In: Auras R, Lim L, Selke S, Tsuji H, editors. Rheology of poly(lactic acid), in poly(lactic acid): synthesis, structures, properties, processing, and applications. Wiley Series; 2010. p. 125−39. Chapter 10.
[20] Grijpma DW, Pennings AJ. Macromol Chem Phys 1994;195:1649−63.
[21] Berger LL. Macromolecules 1989;22:3162−7.
[22] Bhardwaj Rahul, Mohanty Amar K. Biomacromolecules 2007;8:2476−84.
[23] Zhao Q, Ding Y, Yang B, Ning N, Fu Q. Polym Test 2013;32:299−305.
[24] Chan CM, Wu J, Li JX, Cheung YK. Polymer 2002;43:2981−92.
[25] Ljungberg N, Wesslen B. Biomacromolecules 2005;6:1789−96.
[26] Jin HJ, Chin IJ, Kim MN, Kim SH, Yoon JS. Blending of poly(L-lactic acid) with poly(cis-1,4-isoprene). Eur Polym J 2000;36:165−9.
[27] Chow TS. J Polym Sci Polym Phys 1982;20:2103−9.
[28] Zuiderduin WCJ, Westzaan C, Huétink J, Gaymans RJ. Polymer 2003;44:261−75.
[29] Kim GM, Michler GH. Polymer 1998;39:5689−97.
[30] Kim GM, Michler GH. Polymer 1998;39:5699−703.
[31] Meng B, Tao J, Deng J, Wu Z, Yang M. Mater Lett 2011;65:729−32.
[32] Brostow W (editor). Performance of plastics. Hanser (SPE); p. 34.
[33] Lazerri A, Thio YS, Cohen RE. J Appl Polym Sci 2004;91:925−35.
[34] Lazerri A, Bucknall CB. Polymer 1995;36:2895−902.
[35] Argon AS, Cohen RE. Polymer 2003;44:6013−32.
[36] Tandon GP, Weng GJ. Polym Compos 1984;5:327−33.
[37] Parsons EM, Boyce MC, Parks DM, Weinberg M. Polymer 2005;46:2257−65.
[38] Wu S. J Appl Polym Sci 1988;35:549−61.
[39] Maxwell MA, Yee AF. Polym Eng Sci 1981;21:205−11.
[40] Sarvestani AS, Picu CR. Polymer 2004;45:7779−90.
[41] Havet G, Isayev AI. Rheol Acta 2003;42:47−55.
[42] Luo YB, Li WD, Wang XL, Xu DY, Wang YZ. Acta Mater 2009;57:3182−91.
[43] Lin Y, Zhang KY, Dong ZM, Dong LS, Li YS. Macromolecules 2007;40:6257−67.
[44] Huang L, Joshi KL, Van Duin ACT, Bandosz TJ, Gubbins KE. Phys Chem Chem Phys 2012;14:11327−32.